Ionic-Strength Dependence of the Conformational Change in the Unphosphorylated Sodium Pump†

Shwu-Hwa Lin and Larry D. Faller*

CURE: Digestive Diseases Research Center, Department of Medicine, School of Medicine, and Department of Physiological Science, University of California at Los Angeles, and Veterans Administration Greater Los Angeles Health Care System, Los Angeles, California 90073

Received March 5, 2004; Revised Manuscript Received October 14, 2004

ABSTRACT: The conformational change in the unphosphorylated sodium pump was studied as a function of ionic strength to learn whether the rate of the reaction is affected. The results corroborate our proposal [Smirnova, I. N., Lin, S.-H., and Faller, L. D. (1995) *Biochemistry 34,* 8657−8667] that competitive binding of the transported ions to two (or more) equivalent sites regulates a concerted change in protein conformation. An approximately 10-fold increase in ionic strength decreased the intrinsic affinity of the Na^+ conformation of the enzyme for both Na^+ and K^+ roughly 3-fold, decreased the rate of the change from Na^+ to K^+ conformation by more than half, and increased the rate of the reverse reaction by about an order of magnitude. The logarithm of the first-order rate constant for the change from Na^+ to K^+ conformation depended inversely upon the square root of the ionic strength with the extrapolated value at zero ionic strength expressed as a second-order rate constant (1.1×10^9 M^{-1} sec^{-1}) approaching the limit for a diffusion-controlled reaction. The first-order rate constant for the change from K^+ to Na^+ conformation depended directly upon ionic strength and extrapolated to a zero-ionic-strength value (0.002 s^{-1}) far below the diffusion limit. The results are compatible with shielding of oppositely charged domains that move through the solvent when the pump cycles between conformations. Electrostatic interactions between domains evidently contribute to the driving force for the change from Na^+ to K^+ conformation and to the stability of the K^+ conformation.

The working hypothesis for nearly 40 years has been that ion transport by the class of pumps forming a phosphoenzyme intermediate (P-type pumps)[1] results from changed substrate specificity and reoriented ion-binding sites because of a protein rearrangement (*1*, *2*). Today, the structural change can be visualized by viewing an animation[2] based on crystallographic snapshots of Ca-ATPase in two dramatically different conformations (*3*, *4*). In the interim, dynamic studies determined the rate of the reaction and established that binding of the transported ions regulates the conformational change (*5*). The exact mechanism in the first half of the reaction cycle remains uncertain because phosphorylation is coupled to the conformational change, complicating derivation of the rate equation and forcing investigators to resort to numerical simulation (*6*). In contrast, the conformational change in unphosphorylated enzyme during the second half of the reaction cycle is simple enough for rigorous study.

We proposed a concerted mechanism for the rate-limiting conformational change in the unphosphorylated sodium pump (*7*) that explains the stoichiometry of K^+ transport by requiring occupation of two identical and independent sites before the protein rearranges. The model explains reversal of the conformational change by Na^+ competition for the same sites. The predicted dependencies of both the reaction rate and the equilibrium distribution of protein conformers on the Na^+ and K^+ concentration were demonstrated with enzyme covalently labeled with fluorescein by fluorescein 5′-isothiocyanate (FITC). Poor fits of the derived rate and amplitude equations to the experimental data ruled out alternative mechanisms, such as noncompetitive binding (*ibid.*, Figure 2a) or sequential binding without forming metal hybrids with Na^+ and K^+ simultaneously bound (*op. cit.*, Figure 4a). Indistinguishable results were obtained when the conformational change was followed with a noncovalently

† A Veterans Administration Merit Review Award (to L.D.F.) and National Institutes of Health Grant DK52802 (to L.D.F.) supported this research.

* To whom correspondence should be addressed: Telephone: (310) 268-3896. Fax: (310) 268-4963. E-mail: lfaller@ucla.edu.

[1] Abbreviations: Ca-ATPase, calcium pump; Ca^{2+}- and Mg^{2+}-dependent ATPase, EC 3.6.1.38; H,K-ATPase, proton pump; Mg^{2+}-dependent, H^+-transporting, and K^+-stimulated ATPase, EC 3.6.1.36; Na,K-ATPase, sodium pump; Mg^{2+}-dependent and Na^+- and K^+-stimulated ATPase, EC 3.6.1.37; E_{Na}, Na^+ conformation of sodium pump frequently denoted E_1; E_K, K^+ or E_2 conformation; P type, class of pumps forming a phosphoenzyme intermediate; AXP, adenosine 5′-di(D)- or tri(T)phosphate; $Co(NH_3)_4ADP$, α,β-bidentate complex of Co^{3+}, NH_3, and ADP; P_i, inorganic phosphate; eosin, eosin Y (2′,4′,5′,7′-tetrabromofluorescein); FITC, fluorescein 5′-isothiocyanate; RH421, *N*-(4-sulfobutyl)-4-(4-(4-(dipentylamino)phenyl) butadienyl)pyridinium, inner salt; CDTA, *trans*-1,2-diamino-cyclohexane-*N*,*N*,*N*′,*N*′-tetraacetic acid; EDTA, ethylenediaminetetraacetic acid; Tris (Tris$^+$), tris(hydroxymethyl)aminomethane; histidine$^+$, $C_6N_3O_2H_{10}$; ChoCl, choline (Cho^+) chloride; SDS, sodium dodecyl sulfate; SR, sarcoplasmic reticulum; SERCA1, SR fast-twitch skeletal muscle isoform; *R*, correlation coefficient; DeepView, Swiss Protein Data Bank Viewer (us.expasy.org/spdbv); MSA, multiple-sequence alignment; PDB, Protein Data Bank.

[2] www.nature.com/nature/journal/v418/n6896/estref/nature/0094-s3.htm.

10.1021/bi040018c CCC: $30.25
Published on Web 01/11/2005

bound (*8*) or membrane-absorbed (*9*) fluorescent reporter group or energy transfer (*10*), strengthening the evidence for the concerted mechanism.

In the cited series of papers from this laboratory (*7*−*10*), all of the observations in the literature that differed from the predictions of the concerted mechanism were reproduced and explained. For example, an increase in the first-order rate constant was observed with eosin Y (2′,4′,5′,7′-tetrabromofluorescein) (eosin) when enzyme in the K^+ conformation was titrated with Na^+ (*11*). However, at each point in that titration, equal volumes of enzyme and NaCl solutions were mixed without keeping the ionic strength constant. When a neutral salt was used to prevent a simultaneous change in ionic strength, the observed first-order rate constant reported by eosin depended inversely on Na^+ as predicted by the concerted mechanism (*8*). A recent claim that Na^+ accelerates the transition from K^+ to Na^+ conformation by binding to the K^+ conformer is also based on a titration in which Na^+ concentration and ionic strength were simultaneously perturbed by mixing membrane suspensions of the enzyme containing the styryl dye *N*-(4-sulfobutyl)-4-(4-(4-(dipentylamino)phenyl) butadienyl)pyridinium, inner salt (RH421) with equal volumes of salt solutions (*12*). The authors proposed an "induced-fit" mechanism to explain the observed increase in the first-order rate constant with Na^+, citing as support the experiments with eosin in which ionic strength also varied. However, we had shown that the rate of the reaction reported by RH421 at constant ionic strength depends inversely on Na^+ as predicted by the concerted mechanism (*9*).

The experiments described in this paper show that both the forward and reverse rate constants for the conformational change in the unphosphorylated sodium pump (Na,K-ATPase) depend on ionic strength. The effects of ionic strength are compatible with shielding of unlike-charged domains when the pump cycles between "open" and "closed" conformations, such as the Ca^{2+}-bound (*3*) and Ca^{2+}-free (*4*) structures of Ca-ATPase, with interdomain bonds stabilizing the closed conformer.

EXPERIMENTAL PROCEDURES

Materials: FITC-Labeled Enzyme. Membrane fragments containing Na,K-ATPase were isolated from pig kidneys, extracted with sodium dodecyl sulfate (SDS), covalently labeled with FITC, and stored at −80 °C suspended in 50 mM tris(hydroxymethyl)aminomethane (Tris)-HCl containing 1 mM Tris-ethylenediaminetetraacetic acid (EDTA) titrated to pH 7.4 as previously described (*13*). More than one amino acid in Na,K-ATPase reacts with FITC (*14*, *15*), but we showed that the different reactions reported by fluorescein are resolved on the time axis of a stopped-flow experiment (*16*). Only the conformational change reported by fluorescein at an antibody-inaccessible site (*17*) is observed, if the ionic strength (μ) does not change.

Reagents. Fresh pig kidneys were a gift from Farmer John Clougherty Packing Company (Los Angeles, CA). FITC (isomer I) was purchased from Molecular Probes Incorporated (Eugene, OR), and the chloride salts of choline, potassium, and sodium were purchased from Sigma (St. Louis, MO). All other reagents were the highest grade affordable.

General Methods: Stopped-Flow Measurements. The instrument used to make stopped-flow measurements and the protocols for fluorescence-quench and fluorescence-enhancement experiments with FITC-modified Na,K-ATPase were described in detail in earlier publications (*7*, *13*, *16*). The time required to mix two solutions is called the dead time (t_d) and equaled 2.2 ± 0.7 ms for mixing 100 μL aliquots with a drive pressure of 7 bar in our instrument (*18*). The titrant in a quench experiment is K^+, whereas the titrant in an enhancement experiment is Na^+. From 2 to as many as 11 measurements were made at each titrant concentration with most experimental points representing the mean of between 6 and 8 measurements. With one exception in which the buffer concentrations were different, the contents of the enzyme and titrant syringes were identical except for the reactants, 0.13 mM Tris-EDTA in the enzyme syringe and choline chloride (ChoCl), which was varied to keep μ constant. Although ChoCl is not an entirely neutral salt because Cho^+ enhances the fluorescence of FITC-labeled Na,K-ATPase in histidine buffer (*19*), Cho^+ is "unselective" compared to transported ions. Unselective cations such as Cho^+, $Tris^+$, or $C_6N_3O_2H_{10}$ (histidine$^+$) do not affect the fluorescence of bound fluorescein when K^+ or Na^+ is present (*16*). K^+ and Na^+ were also added as chloride salts, so that the anion concentration did not change. The contribution of EDTA to μ was estimated with a program for calculating free chelator and ligand concentrations called "bound and determined" (*20*), and literature values of the $pK_a = 8.3$ at 20 °C and $\Delta pK_a/°C = -0.031$ for Tris were used to calculate the contribution of the buffer (*21*). Ionic strengths are quoted to the nearest 0.5 mM. Specific protocols for an example of each type of experiment, including the exception in which mixing also changed the Tris-HCl concentration slightly, are given in the figure captions. The fluorescence quench and enhancement were titrated by incrementing the independent variable (Na^+ or K^+) with μ fixed at different values.

Data Analysis. An advantage of stopped-flow measurements is that both kinetic and equilibrium data are obtained from the same experiment. An empirical pseudo-first-order rate constant and the amplitude of the fluorescence change were estimated by fitting eq 1 for exponential time dependence with an offset (i.e., nonzero endpoint) to recordings of voltage, which is proportional to fluorescence intensity (F) in arbitrary units (au), versus time (t). In eq 1, the pseudo-

$$F = \Delta F_d e^{-t/\tau} + F_\infty \quad (1)$$

first-order rate constant is written as the reciprocal of the relaxation time (τ), which is the time required for the fluorescence intensity to decay to approximately one-third of its initial value. F is the observed fluorescence intensity; F_∞ is the estimated fluorescence at infinite time; and $\Delta F_d = F_d - F_\infty$ is the amplitude of the observed fluorescence change. F_d is the estimated fluorescence at the start of the observations ($t = 0$), which are triggered by stopping flow; therefore, ΔF_d is significantly less than the actual fluorescence change ($\Delta F_0 = F_0 - F_\infty$), where F_0 is the fluorescence intensity at the start of mixing, if τ is small compared to t_d (see Figure 1 in ref *19*). Therefore, the estimated K^+-quench amplitudes were corrected with eq 2. The inverse of τ or

$$\Delta F_0 = \Delta F_d e^{t_d/\tau} \quad (2)$$

the corrected maximum (equilibrium) fluorescence change (ΔF_0) expressed as a percentage of F_∞ was plotted as a function of the independent variable. Thinking of stopped-flow measurements as relaxation experiments emphasizes that $1/\tau$ is not a constant and simplifies derivation of the rate equation (appendix of ref *18*), which shows the dependence of $1/\tau$ on the monovalent cation concentrations, the intrinsic or microscopic K^+ (K_K) and Na^+ (K_{Na}) dissociation constants from the Na^+ conformation, and the forward (k_f) and reverse (k_r) rate constants for the protein conformational change with direction defined by writing the Na^+ conformation detected by fluorescence or energy transfer (E_{Na}) on the left and the K^+ conformation detected by the same techniques (E_K) on the right in the chemical equation for the partial reaction $E_{Na}K_2 \rightleftharpoons E_KK_2$. (*7*).

Concerted Mechanism. Environment-sensitive fluorescent probes were shown to report a rate-limiting conformational change by superimposing data obtained with fluorescein and eosin on energy-transfer data reporting a change in distance between two specifically labeled points on the protein (*10*). The magnitude of the distance change estimated from energy transfer (2.9 ± 0.6 Å) is consistent with observed changes in distance between comparable points (0.68−2.49 Å) in the crystal structures of Ca-ATPase with (*3*) and without (*4*) Ca^{2+} bound. If the conformational change is regulated by competition of the transported ions for two identical and independent sites on E_{Na} (*7*), eq 3 is the relaxation expression. Kinetic

$$\frac{1}{\tau} = k_f\left[\frac{[K^+]}{[K^+] + K_K\left(1 + \frac{[Na^+]}{K_{Na}}\right)}\right]^2 + k_r \qquad (3)$$

titrations of Na,K-ATPase with K^+ extrapolate to k_f because $k_f \gg k_r$ (*13*) and the shape of the curve depends only on K_K when Na^+ is absent. Conversely, kinetic titrations with Na^+ extrapolate to k_r. Equations for predicting the half-maximum molar titrant concentrations of kinetic K^+-quench ($[K^+]_{1/2}$) and Na^+-enhancement ($[Na^+]_{1/2}$) experiments were published in ref *7* (eqs 3 and 4). The instrument dead time-corrected amplitude of a stopped-flow trace (F versus t) is the fluorescence change that would be observed in an equilibrium titration reporting only the conformational change. Equation 4 is the expression for the fractional change in amplitude of the K^+ quench when Na^+ is omitted and the enzyme starts out as E_{Na}. Equation 5 is the expression for the fractional

$$\frac{\Delta F_o}{F_\infty} = \frac{[K^+]^2}{[K^+]^2 + \frac{2K_K}{(1+K_c)}[K^+] + \frac{{K_K}^2}{(1+K_c)}} \frac{K_c}{(1+K_c)} \frac{\Delta F_{max}}{F_\infty} \qquad (4)$$

change in amplitude of the Na^+ enhancement when the enzyme starts out as E_K and $[K^+]$ does not change. In eqs 4 and 5, K_c is the equilibrium constant for the change from E_{Na} to E_K conformation (k_f/k_r) and ΔF_{max} is the difference in fluorescence intensity between E_{Na} and E_K. Reference *7* contains equations (eqs 8 and 9) for predicting $[K^+]_{1/2}$ and $[Na^+]_{1/2}$ for equilibrium-amplitude titrations. Equation 3 was fitted to $1/\tau$ data for titrations with K^+ ($[Na^+] = 0$) to estimate k_f and K_K, which were fixed when eq 3 was fitted to $1/\tau$ data for titrations with Na^+ to estimate k_r and K_{Na}. Estimates of $\Delta F_{max}/F_\infty$ and equilibrium estimates of K_K and K_{Na} were obtained by fitting eq 4 to the amplitude data for the K^+ quench with k_f and k_r fixed and by fitting eq 5 to amplitude data for the Na^+ enhancement with $[K^+]$, k_f, K_K, and k_r fixed.

$$-\frac{\Delta F_o}{F_\infty} = \left\{\left[[Na^+]^2 + 2K_{Na}\left(1 + \frac{[K^+]}{K_K}\right)[Na^+]\right] \Big/ \left[[Na^+]^2 + 2K_{Na}\left(1 + \frac{[K^+]}{K_K}\right)[Na^+] + {K_{Na}}^2\left[\left(1 + \frac{[K^+]}{K_K}\right)^2 + K_c\left(\frac{[K^+]}{K_K}\right)^2\right]\right]\right\} \frac{[K^+]^2}{[K^+]^2 + \frac{2K_K}{(1+K_c)}[K^+] + \frac{{K_K}^2}{(1+K_c)}} \times \frac{K_c}{1+K_c}\frac{\Delta F_{max}}{F_\infty} \qquad (5)$$

Homology Modeling. Models of the Na^+ and K^+ conformations of the sodium pump were obtained by submitting a manually edited multiple-sequence alignment (MSA) of the pig α1 subunit (Swiss-Prot accession number P05024) with six other P-type pumps (P58312, P13607, P19156, P04191, P11607, and Q9XES1) to the Swiss-model server with the Ca^{2+}-bound [Protein Data Bank (PDB) identifier 1EUL] and Ca^{2+}-free (1IWO) structures of Ca-ATPase as the templates. The MSA was edited by aligning S488 of the template sarcoplasmic reticulum (SR) fast-twitch skeletal muscle isoform (SERCA1) sequence with S482 of the target Na,K-ATPase sequence, so that a one amino acid gap follows F487 instead of K492 in the SERCA1 sequence.

RESULTS

K^+ Quench. Figure 1 compares experiments in which the same $[K^+]$ was mixed with FITC-labeled enzyme in the Na^+ conformation at two different ionic strengths. The reactant (enzyme and titrant) solutions contained $Tris^+$ and Cho^+, which shift the equilibrium between E_{Na} and E_K toward E_{Na} (*16*, *19*), and were identical except for the reactants and for the amount of ChoCl needed to fix μ at different values. The residual plot shows that single exponentials satisfactorily fit both kinetic traces. The rate increase caused by decreasing μ calculated from the $1/\tau$ estimates reported in the figure caption was (1.54 ± 0.06)-fold for a final $[K^+]$ of 1 mM.

Na^+ Enhancement. Figure 2 shows the effect of μ on reversal of the K^+ quench by Na^+. Experiments at the highest Na^+ concentrations experimentally feasible are compared to minimize the contribution of the first term in eq 3 containing $[K^+]$ to the observed $1/\tau$. More K^+ was needed to convert the enzyme to E_K at the higher ionic strength. Therefore, more Na^+ was needed and could be used to reverse the conformational change without changing μ. The only other differences were the ChoCl concentrations required to achieve different ionic strengths and the concentration of buffer. In contrast to the quench reaction, the enhancement reaction is visibly faster at the higher ionic strength. The rate increase caused by increasing μ calculated from the $1/\tau$ estimates reported in the figure caption was (2.70 ± 0.07)-fold.

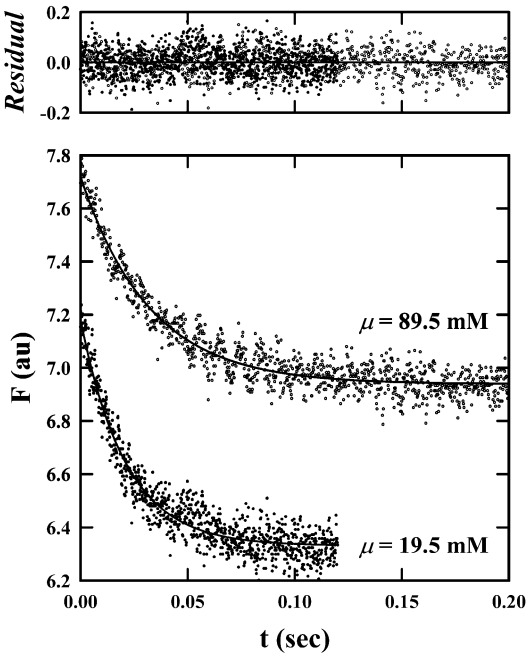

FIGURE 1: Comparison of K^+-quench experiments at different ionic strengths. Fluorescence (F) in arbitrary units (au) is plotted against time (t) in seconds with 0.6 au subtracted from each measured point in the $\mu = 19.5$ mM experiment to separate the curves. Each stippled trace is a single experiment in which equal volumes (100 μL) of a membrane suspension of the enzyme and a titrant solution were mixed at 15 °C with a drive pressure of 7 bar, and 1001 data points were collected. The enzyme syringe contained 0.15 mg mL^{-1} protein in 0.13 mM Tris-EDTA from the stock membrane suspension and 10 mM ($\mu = 19.5$ mM) or 80 mM ($\mu = 89.5$ mM) ChoCl buffered by 10 mM Tris-HCl at pH 7.4. The titrant syringe contained 2 mM KCl and 8 mM ($\mu = 19.5$ mM) or 78 mM ($\mu = 89.5$ mM) ChoCl in 10 mM Tris-HCl (pH 7.4). The solid lines are fits of eq 1 to the experimental data. The parameter estimates from the $\mu = 19.5$ mM data (●) were $1/\tau = 47.6 \pm 0.9$ s^{-1}, $\Delta F_d = 0.853 \pm 0.008$ au, and $F_\infty = 6.330 \pm 0.003$ au, and the corresponding values for the $\mu = 89.5$ mM data (○) were $1/\tau = 31.0 \pm 0.6$ s^{-1}, $\Delta F_d = 0.781 \pm 0.008$ au, and $F_\infty = 6.939 \pm 0.003$ au. The residual plot shows the difference between the fitted and observed fluorescence intensities at each time point in the $\mu = 19.5$ or 89.5 mM experiments.

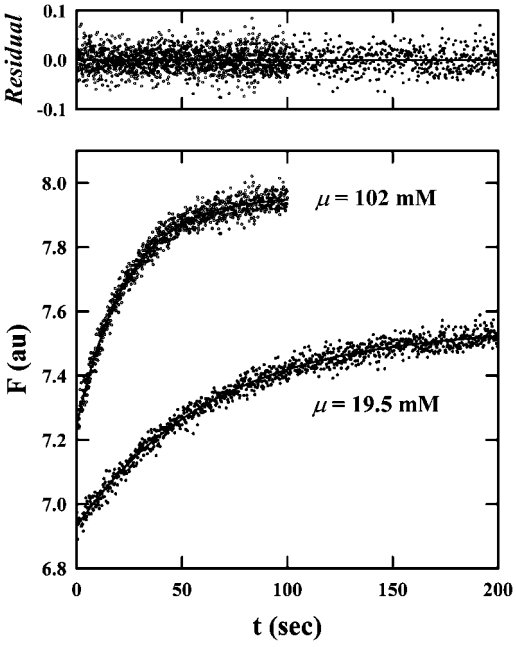

FIGURE 2: Comparison of Na^+-enhancement experiments at different ionic strengths. Reversal of the fluorescence quench by Na^+ at two ionic strengths is plotted against time with 0.4 au added to the observed fluorescence intensity at every time point in the $\mu = 102$ mM curve to separate the data. The instrument settings were the same as in Figure 1. However, the enzyme syringe contained 0.15 mg mL^{-1} protein in 0.13 mM Tris-EDTA, 0.1 mM KCl, 9.9 mM ChoCl, and 10 mM Tris-HCl (pH 7.4), and the titrant syringe contained 0.1 mM KCl, 0.1 mM ChoCl, 9.8 mM NaCl, and 10 mM Tris-HCl (pH 7.4) in the $\mu = 19.5$ mM experiment. In the $\mu = 102$ mM experiment, 0.15 mg mL^{-1} protein in 0.13 mM Tris-EDTA, 1 mM KCl, 79 mM ChoCl, and 27 mM Tris-HCl (pH 7.4) was mixed with 1 mM KCl and 79 mM NaCl in 20 mM Tris-HCl at pH 7.4. The solid lines are the fits of eq 1 to the data with parameter estimates of $1/\tau = 0.0156 \pm 0.0002$ s^{-1}, $\Delta F_d = -0.620 \pm 0.003$ au, and $F_\infty = 7.550 \pm 0.002$ au for the $\mu = 19.5$ mM data (●) and $1/\tau = 0.0421 \pm 0.0005$ s^{-1}, $\Delta F_d = -0.716 \pm 0.003$ au, and $F_\infty = 7.958 \pm 0.002$ au for the $\mu = 102$ mM data (○). The residual plot shows the deviations of the experimental points from the fitted lines in the $\mu = 19.5$ and 102 mM experiments.

K^+ Titration. Figure 3 shows the dependence of $1/\tau$ for the K^+ quench on $[K^+]$ as a function of μ. In this figure and the three that follow, triangles (19.5 mM), circles (89.5 or 102 mM), and squares (246 mM) denote titrations at different ionic strengths. The error bars represent the standard deviation in the mean of n individual estimates of $1/\tau$, which is larger than the standard deviation in the estimate of $1/\tau$ found by summing the data from n measurements, dividing by n, and fitting the averaged data. For example, the 8 individual estimates of $1/\tau$ for the titration with 2 mM K^+ and $\mu = 19.5$ mM shown in Figure 1 were 97.9, 98.3, 96.8, 100.3, 87.9, 102.4, 90.2, and 87.8 s^{-1} giving the mean and standard deviation (95.2 ± 5.7 s^{-1}) plotted in Figure 3. The same estimate of $1/\tau$ was obtained by fitting the averaged data, but the error estimate was only ± 0.9 s^{-1}. The rate decreased when μ was increased at every $[K^+]$, so that kinetic quench-titration curves at higher ionic strengths fall below the corresponding titration curves at lower ionic strengths in Figure 3. The titrant axis is broken to show that $1/\tau$ depended sigmoidally on $[K^+]$ as predicted by the concerted mechanism. The values of k_f and K_K estimated by fitting eq 3 to $1/\tau$ versus $[K^+]$ data and the standard errors in the parameter estimates are reported in Table 1. The estimates of k_r were zero within experimental error. Therefore, the estimates of k_r obtained by fitting eq 3 to $1/\tau$ versus $[Na^+]$ data at the same (▲ and ■) or nearly the same (●) μ (Table 1) were used to calculate the solid lines in Figure 3. Bold in Table 1 indicates the "best" estimates of parameters that were fixed when fitting other titrations. The predicted $[K^+]_{1/2}$ is also reported in column 5, and the estimated correlation coefficient (R) is tabulated as an indication of the quality of the fit (*22*). The probability that from 14 ($\mu = 19.5$ and 246 mM) to 21 ($\mu = 89.5$ mM) mean measurements would give a value of R greater than 0.9 if the variables were unrelated by eq 3 is conservatively less than 5%. The titration curves were also fitted with the equation for sequential binding to two independent but nonidentical sites (*23*), and column 6 reports the ratio of the estimated macroscopic constants for dissociation of K^+ from the sites filled last (K_{K_2}) and first (K_{K_1}).

Figure 4 shows the dependence of the quench amplitude on $[K^+]$. The shapes of the symbols and the error bars have the same meaning as in Figure 3. At each μ, the data were fitted with eq 4, with k_f and k_r fixed at the values shown in bold in Table 1. The solid lines were calculated with the

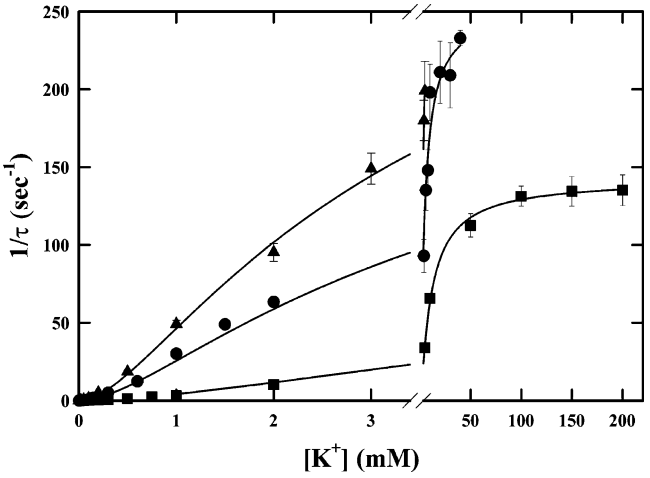

FIGURE 3: Titration of quench rate with K^+. The observed first-order rate constant ($1/\tau$) when μ was 19.5 mM (▲), 89.5 mM (●), or 246 mM (■) is plotted against the final K^+ concentration after mixing. Each point is the mean of from 2 to 11 measurements (Figure 1), with $n = 7$ being the median number of measurements. The error bars indicate the standard deviation in the mean of the n measurements fitted individually with eq 3. The experimental protocol for titrations with $\mu = 19.5$ or 89.5 mM is given in the caption of Figure 1, except that the KCl and ChoCl concentrations in the titrant syringe were varied to give the desired final $[K^+]$. For example, the concentration of KCl in the titrant syringe for the 3 mM K^+ point in the $\mu = 89.5$ mM plot was 6 mM, and the ChoCl concentration was 74 mM. The concentrations of protein and EDTA in the enzyme syringe were the same in the $\mu = 246$ mM titration as in the $\mu = 19.5$ or 89.5 mM experiment, but the Tris-HCl concentration was 50 mM and the ChoCl concentration was 200 mM. The concentration of KCl in the titrant syringe was twice the concentration of K^+ on the abscissa. The sum of the KCl and ChoCl concentrations in the titrant syringe was 200 mM in 50 mM Tris titrated to pH 7.4 with HCl. The solid lines were calculated with the estimates of k_f and K_K obtained by fitting eq 3 to the data with k_r undetermined and k_r obtained by fitting enhancement titrations (Figure 5) for the same or nearly the same μ with k_f and K_K fixed at the quench values. The parameter estimates are summarized in Table 1.

fixed parameters and the estimates of ΔF_{max} and K_K. The concentration axis is broken to show that the data are consistent with sigmoidal dependence of the ΔF_0 on $[K^+]$, although titrations in the presence of Na^+ are required to show the sigmoidicity predicted by eq 4 clearly (see ref *7* and Figure 1b). The parameter estimates are reported in Table 1. The correlation coefficients in column 7 mean that the amplitudes are related to $[K^+]$ by eq 4 at greater than the 95% confidence level. Column 8 is labeled $\Delta F_{max}/F_\infty$, even though only $[K_c/(1 + K_c)]\Delta F_{max}/F_\infty$ can be observed experimentally, because $K_c \gg 1$ (column 6 of Table 1) for the sodium pump. The estimated maximum fluorescence change is roughly the same, even though different enzyme preparations were used in some experiments at different ionic strengths. The estimates of K_K obtained by fitting amplitude titrations with eq 4 (column 9) are not significantly different from those obtained by fitting $1/\tau$ titrations with eq 3 (column 4), and the predicted $[K^+]_{1/2}$ values (column 10) correspond to the observed half-maximum K^+ concentrations in Figure 4.

Na^+ Titration. The reciprocal relaxation times for Na^+ reversal of the fluorescence quench caused by 0.1 mM K^+ (▲), 1 mM K^+ (●), or 5 mM K^+ (■) are plotted against $[Na^+]$ in Figure 5. The K^+ concentrations were chosen to completely convert the enzyme to E_K when μ was 19.5, 89.5, or 246 mM, respectively (Figure 4). Error bars have the same meaning as in Figures 3 and 4. The solid lines are fits of eq 3 to the data with k_f and K_K fixed at the values in bold in Table 1. The estimates of k_r and K_{Na} are reported in Table 1. In contrast to Figure 3 for the quench reaction, kinetic enhancement-titration curves for higher ionic strengths lie above the corresponding titration curves for lower ionic strengths in Figure 5. The estimates of k_r in column 3 are essentially independent of the other parameters because $1/\tau$ asymptotically approaches k_r. However, the uncertainty in the estimates increased as μ was lowered because the maximum $[Na^+]$ that could be used to establish the asymptotic limit without perturbing μ decreased. The uncertainties in k_f and k_r propagate into the calculated equilibrium constant for the conformational change; therefore, the uncertainty in K_c is also inversely related to μ (column 6). The intercepts on the $1/\tau$ axis ($[Na^+] = 0$) predicted with eq 3 and the values of k_f, K_K, and k_r in Table 1 are 0.96 s^{-1} ($\mu = 19.5$ mM), 25 s^{-1} ($\mu = 102$ mM), and 35 s^{-1} ($\mu = 246$ mM). Therefore, only 31% of the titration curve was observed in the best case ($\mu = 19.5$ mM), and the estimates of K_{Na} in column 4, which depend on the shape of the titration curve, are not as certain as implied by the standard errors in K_{Na} estimated from the fits. Nevertheless, the estimates of R in column 2 indicate that $1/\tau$ is related to $[Na^+]$ by eq 3 with greater than 95% probability. The predicted $[Na^+]_{1/2}$ values are reported in column 5 of Table 1.

Figure 6 shows the dependence of the enhancement amplitude on $[Na^+]$. The symbols have the same meaning with respect to both $[K^+]$ and μ as in Figure 5. Equation 5 was fit to the data with k_f, K_K, and k_r fixed at the values in bold in Table 1. The fixed parameter values and parameter estimates were substituted into eq 5 to calculate the solid lines in Figure 6. The concentration axis is broken to show the sigmoidal shape of the titration curves predicted by the concerted mechanism. The estimates of $\Delta F_{max}/F_\infty$ and K_{Na} are reported in Table 1. The values of R in column 7 indicate that the probability of the enhancement amplitude being unrelated to $[Na^+]$ by eq 7 is less than 5%. The maximum percentage change in amplitude (column 8) is practically independent of μ despite using several different labeled-enzyme preparations in the titrations. The estimates of K_{Na} in column 9 are in bold, even though they were not fixed in any fits, to indicate that they are more reliable estimates of K_{Na} than the values in column 4 because there were many more experimental points in the concentration range that determines K_{Na} in the amplitude titration (Figure 6) than in the rate titration (Figure 5). The observed half-maximum Na^+ concentrations agree well with the predicted $[Na^+]_{1/2}$ values (column 10).

Ionic-Strength Titration. In Figure 7, the estimated rate constants for the change from E_{Na} to E_K in Table 1 are plotted against μ. The inset shows that the logarithm of k_f depended linearly upon the square root of μ [correlation coefficient (R) = 0.9990]. The maximum value of k_f ($\mu = 0$) estimated from the intercept of the straight line on the log k_f axis was 586 ± 1 s^{-1}. The dashed line in the plot of k_f versus μ was calculated with the slope and intercept obtained from the straight line in the inset, which are reported in the figure caption.

The estimated rate constants for the change from E_K to E_{Na} (●) are plotted against μ in Figure 8. The solid line

Table 1: Comparison of Kinetic and Equilibrium Parameter Estimates

K^+ Quench

	rate titration					amplitude titration			
μ (mM)	R	k_f (sec^{-1})	K_K (mM)	$[K^+]_{1/2}$	K_{K_2}/K_{K_1}[a]	R	$\Delta F_{max}/F_\infty$ (%)	K_K (mM)	$[K^+]_{1/2}$
19.5	0.9994	**379 ± 14**[b]	**1.9 ± 0.1**	4	4 ± 3	0.9752	11.8 ± 0.3	1.4 ± 0.2	0.01
89.5	0.9957	**254 ± 7**	**2.2 ± 0.2**	5	5 ± 5	0.9894	10.9 ± 0.2	1.9 ± 0.2	0.03
246	0.9995	**142 ± 1**	**5.1 ± 0.2**	12	4 ± 2	0.9939	12.9 ± 0.2	5.8 ± 0.3	0.15

Na^+ Reversal

	rate titration					amplitude titration			
μ (mM)	R	k_r (sec^{-1})	K_{Na} (mM)	$[Na^+]_{1/2}$	K_c ($\times 10^{-3}$)	R	$\Delta F_{max}/F_\infty$ (%)	K_{Na} (mM)	$[Na^+]_{1/2}$
19.5	0.9894	**0.010 ± 0.006**	0.32 ± 0.02	0.1	38 ± 24	0.9979	9.0 ± 0.2	**0.165 ± 0.006**	1.5
102	0.9925	**0.05 ± 0.02**	0.31 ± 0.01	0.2	5 ± 3	0.9996	9.88 ± 0.07	**0.212 ± 0.003**	6.5
246	0.9928	**0.114 ± 0.003**	0.71 ± 0.01	0.6	1.25 ± 0.04	0.9994	8.86 ± 0.04	**0.52 ± 0.01**	17

[a] Ratio of estimated macroscopic dissociation constants for sequential binding of K^+ to two nonidentical K^+ sites (*23*). [b] Bold indicates best estimates of parameters that were fixed, except in one case (K_{Na}), when fitting other titrations.

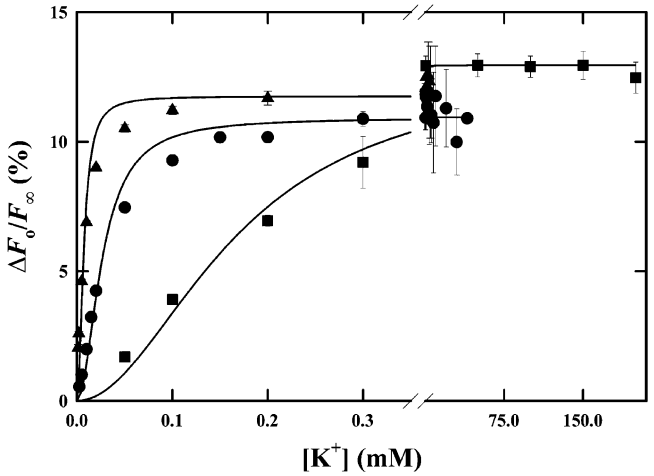

FIGURE 4: Titration of quench amplitude with K^+. The estimated maximum amplitudes (ΔF_d) for the experiments described in Figure 3 with μ = 19.5 mM (▲), 89.5 mM (●), or 246 mM (■), corrected for the dead time of the instrument with eq 2 (ΔF_0) and expressed as a percentage of the fluorescence intensity at infinite time (F_∞), are plotted against the final $[K^+]$ after mixing. The solid lines were calculated with the estimates of $\Delta F_{max}/F_\infty$ and K_K obtained by fitting the data with eq 4 and the values of k_f and k_r for the corresponding μ in bold in Table 1. The values of $\Delta F_{max}/F_\infty$ and K_K estimated from the amplitude data are reported in Table 1.

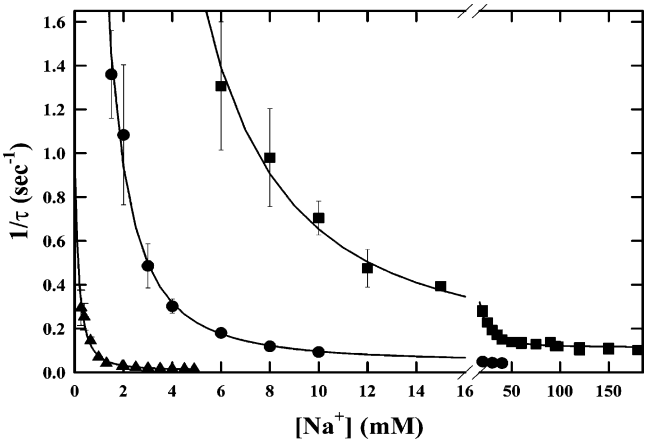

FIGURE 5: Titration of enhancement rate with Na^+. The observed first-order rate constant ($1/\tau$) when μ was 19.5 mM (▲), 102 mM (●), or 246 mM (■) is plotted against the final $[Na^+]$ after mixing. The experimental protocols for measurements with μ = 19.5 or 102 mM are given in the caption of Figure 2, except that the concentrations of NaCl and ChoCl in the titrant syringe were varied to give the desired final $[Na^+]$ without changing μ. The concentrations of protein and EDTA in the enzyme syringe were the same in the μ = 246 mM titration as in the μ = 19.5 or 102 mM experiment, but the enzyme syringe contained 5 mM KCl and 195 mM ChoCl in 50 mM Tris-HCl. The titrant syringe contained 5 mM KCl and twice the NaCl concentration shown on the abscissa. The sum of the KCl, NaCl, and ChoCl concentrations in the titrant syringe was 200 mM in 50 mM Tris titrated to pH 7.4 with HCl. The solid lines were calculated with eq 3 and the values of k_f and K_{Na} estimated by fitting eq 3 to the data with k_f and K_K fixed at the values in bold in Table 1. The parameter estimates are reported in Table 1.

through the points indicates linear dependence of k_r on μ (R = 0.9997). The minimum value of k_r estimated from the intercept on the ordinate axis was 0.0020 ± 0.0016 s^{-1}. The open circles were taken from Figure 6 in ref *11* for comparison. In the cited paper, Na,K-ATPase (0.1 mg mL^{-1}) in 10 mM histidine buffer (pH 7.5) containing 10 mM *trans*-1,2-diamino-cyclohexane-*N*,*N*,*N*′,*N*′-tetraacetic acid (CDTA), 0.5 μM eosin, and 0.05 mM RbCl was mixed with the same buffer containing from 50 to 900 mM NaCl at 20 °C. The observed first-order rate constant (k_{obs}), which is equivalent to $1/\tau$ in eq 1, for converting the enzyme to E_{Na} is plotted against the final ionic strength, obtained by adding the estimated ionic strength of 10 mM histidine (pH 7.5) containing 1 mM CDTA and 0.05 mM RbCl to one-half of the NaCl concentration. Literature values for ionization of histidine (*21*) and CDTA (*24*) were used to estimate the contribution of the buffer to μ (16 mM). The dashed line, calculated for a linear relationship between $1/\tau$ and μ (R = 0.9960), gave a minimum estimate for the ordinate intercept of 0.008 ± 0.005 s^{-1}.

DISCUSSION

The rates of bimolecular reactions between charged molecules in solution are normally affected by ionic strength because ions present in solution shield the charges on the molecules (*25*). The effects of μ on diffusion-controlled rates of association and dissociation are reversed with the direction of the change depending upon whether the reactants have charges of the same or opposite sign. For example, the rate of association of oppositely charged molecules decreases with increasing μ because the ionic atmosphere reduces the electrostatic attraction. Conversely, the rate of dissociation increases with μ because shielding makes it easier to separate unlike charges. Therefore, the dissociation constant (dissociation rate constant over association rate constant) of a

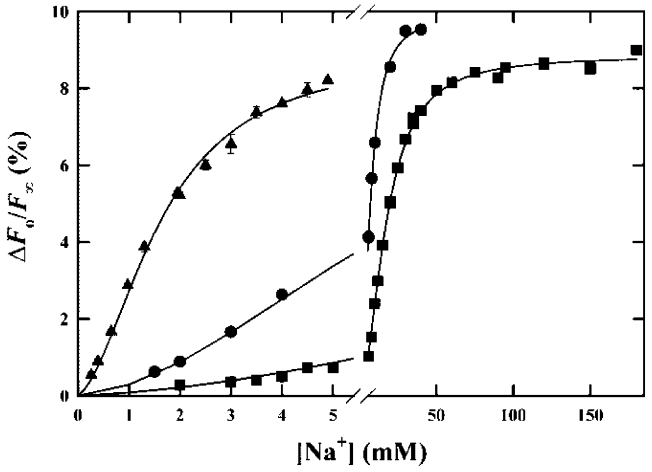

FIGURE 6: Titration of enhancement amplitude with Na^+. The corrected amplitudes (ΔF_0), which equaled the observed maximum amplitudes (ΔF_d) because $\tau > t_d$ for the experiments shown in Figure 5 with $\mu = 19.5$ mM (▲), 102 mM (●), or 246 mM (■), are plotted against the final [Na^+] after mixing. The solid lines were calculated with the estimates of $\Delta F_{max}/F_\infty$ and K_{Na} obtained by fitting the data with eq 5 and the values of k_f, K_K, and k_r in bold in Table 1. The estimates of $\Delta F_{max}/F_\infty$ and K_{Na} obtained from the enhancement amplitude data are reported in Table 1.

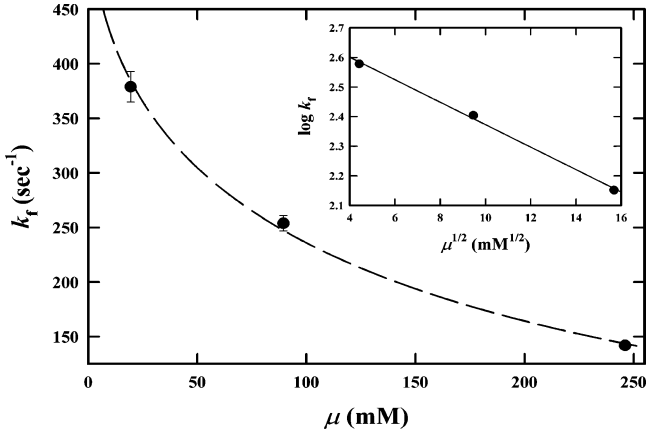

FIGURE 7: Titration of k_f with ionic strength. The estimates of k_f in bold in Table 1 are plotted against ionic strength. The error bars indicate the standard errors in the estimates. The inset is a plot of the logarithm of k_f versus the square root of μ. The solid line in the inset is the fit of eq 6 to the data ($R = 0.9990$). The dashed line in the plot of k_f versus μ was calculated with the slope (-0.038 ± 0.002 mM$^{1/2}$) and intercept (2.75 ± 0.02) of the straight line in the inset.

complex between unlike-charged molecules increases with increasing μ.

Unimolecular reactions may not be affected by μ, but the conformational change in P-type pumps involves large domain movements. We estimated a distance of as much as 26 Å between fluorescein covalently bound to the nucleotide site of Na,K-ATPase and $Co(NH_3)_4ADP$, which is a competitive inhibitor of phosphorylation by inorganic phosphate (P_i), from energy-transfer measurements (*26*). The open structure of Ca-ATPase with Ca^{2+} bound confirmed that the phosphorylation site in P-type pumps is more than 25 Å away from the nucleotide site (*3*). Large movements of the cytosolic nucleotide, phosphorylation, and N-terminal domains were demonstrated by the recently published closed structure of Ca-ATPase without Ca^{2+} bound (*4*). The Ca^{2+}-bound and Ca^{2+}-free structures of Ca-ATPase presumably

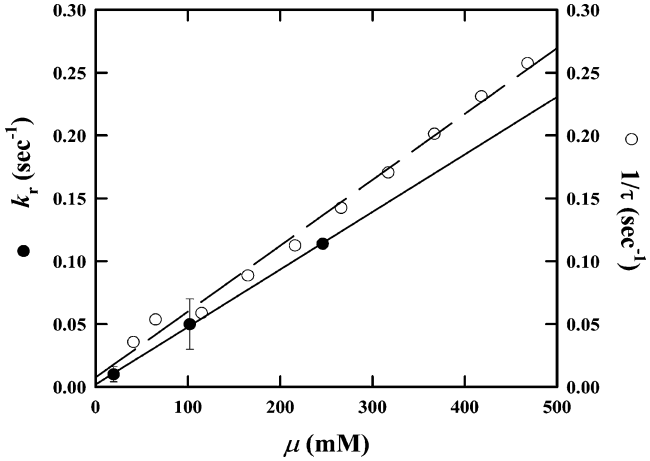

FIGURE 8: Titration of k_r with ionic strength. The estimates of k_r in bold in Table 1 (●) are plotted against μ. The solid line was calculated for a linear relationship between k_r and μ with the slope ($4.6 \pm 0.1 \times 10^{-4}$ mM^{-1} sec^{-1}) and intercept ($2.0 \pm 1.6 \times 10^{-3}$ sec^{-1}). The k_{obs} values (○), which are equivalent to $1/\tau$ in eq 2, were taken from the literature (*11*). The dashed straight line through the open circles was calculated with estimates of $5.2 \pm 0.2 \times 10^{-4}$ mM^{-1} sec^{-1} for the slope and $8 \pm 5 \times 10^{-3}$ sec^{-1} for the ordinate intercept. The differences between the experimental designs of the experiments used to obtain k_r and k_{obs} are explained in the text.

correspond to the Na^+ and K^+ conformations of Na,K-ATPase, respectively. Therefore, the rate of the conformational change in P-type pumps could depend on μ, if electrostatic interactions contribute to the driving force for the domain movements and stabilization of the closed structure. Figure 1 shows unambiguously that increasing μ decreased the rate of the change from E_{Na} to E_K because the only difference between the experiments was μ. The interpretation of Figure 2 depends on the mechanism of the reaction because experiments at different final Na^+ and K^+ concentrations are compared. Therefore, corroboration of the concerted mechanism by the ionic strength data is discussed, and evidence in the literature for alternative mechanisms is refuted before turning to the implications of dependence on μ for the molecular mechanism of the conformational change in P-type pumps.

Corroboration of Concerted Mechanism. More than one site on Na,K-ATPase for both Na^+ and K^+ was required to explain sigmoidal titration curves for the conformational change at roughly physiological μ (*7*, *23*). Two inflections are unmistakable in both the kinetic titration with K^+ (Figure 3) and in the equilibrium titration with Na^+ (Figure 6) at lower ionic strengths as well. The justification for describing binding to multiple sites on E_{Na} by a single microscopic dissociation constant was that the ratio of the macroscopic constants estimated for sequential binding to two sites was the expected value (four) for random binding (*27*) of both Na^+ and K^+ independent of the enzyme preparation (*7*) and of an intrinsic property of the system temperature (*19*). Column 6 of Table 1 strengthens the evidence for binding to identical and independent sites by showing that the ratio K_{K_2}/K_{K_1} also equaled 4, within experimental error, independent of the extrinsic property ionic strength. The predicted (eq 3) increase in $1/\tau$ with [K^+] and decrease in $1/\tau$ with [Na^+] are demonstrated in Figures 3 and 5 for different ionic strengths. The reason for larger estimates of $\Delta F_{max}/F_\infty$ from amplitude titrations with K^+ (Table 1) than those with Na^+ (Table 1) is that the maximum fluorescence change is

expressed as a percentage of F_∞ to permit comparison of titrations; therefore, the endpoints of titrations with Na^+ and K^+ are different. The endpoint of a titration with K^+ is the fluorescence intensity of E_K, whereas the endpoint of a titration with Na^+ is the fluorescence intensity of E_{Na}, which equals the fluorescence intensity of E_K plus the difference in fluorescence intensity between E_K and E_{Na}. The K^+ quench was completely reversed by Na^+, when the difference in endpoints is taken into account. The solid lines in Figures 3−6 and the correlation coefficients in Table 1 show that the equations derived for the concerted mechanism satisfactorily fit both rate and amplitude data as a function of both $[Na^+]$ and $[K^+]$ at all ionic strengths. The values of K_K and K_{Na} in Table 1 estimated from kinetic and equilibrium titrations are not significantly different. A limitation of kinetic studies is that experimental data can always be fit equally well by more complicated mechanisms than the simplest required mechanism. Therefore, anticooperative binding to two sites fortuitously differing in affinity for both Na^+ and K^+ by a factor of 4 cannot be ruled out. Only two sites are needed to explain the ionic-strength data as well as earlier results obtained with fluorescein, eosin, RH421, and energy transfer, but three sites consistent with stoichiometric evidence for three Na^+ sites and electrogenic countertransport of two K^+ ions fit the data equally well (*7*).

Refutation of Evidence for Alternative Mechanisms. Any effect of μ on the rate of the change from E_{Na} to E_K was masked in published titrations with K^+ from other laboratories because K^+ and μ were simultaneously varied (*28*−*30*). The estimates of k_f in Table 1 are not as precise as implied by the reported standard deviations, which were estimated by fitting the individual titration curves in Figure 3. However, a more realistic estimate of the uncertainty (±19 s^{-1}) in the mean value of k_f (150 s^{-1}) at the highest μ (246 mM) from a larger array of data (i.e., ±13%), in which $[Na^+]$ as well as $[K^+]$ was varied (*7*), supports the conclusion that k_f increased significantly (>2-fold) when μ decreased (Figure 7).

To strengthen the conclusion that k_r depends directly upon μ, published data (○) from a different laboratory obtained using a different fluorescent reporter group (*11*) are plotted along with the estimates of k_r from Table 1 (●) in Figure 8. The pseudo-first-order rate constant (k_{obs}) measured with eosin is equivalent to $1/\tau$ in eq 3. Rubidium (0.05 mM), instead of K^+, was used to shift the enzyme to the conformation with lower fluorescence intensity. The Rb^+ dissociation constant was not measured; therefore, the contribution of the first term in eq 3 to the observed first-order constant cannot be calculated exactly. However, the first term in eq 3 calculated for the corresponding $[K^+]$ (0.05 mM) and the lowest $[Na^+]$ (25 mM) in the eosin titration with the parameter estimates in bold in Table 1 (1×10^{-5} sec^{-1}) would not increase $1/\tau$ significantly above our estimate of k_r (0.01 s^{-1}) at the lowest μ (19.5 mM), where k_f was largest. Therefore, k_{obs} probably equaled k_r in the eosin experiments also. The values of k_r obtained by extrapolating the straight lines in Figure 8 to 0 μ are (0.008 ± 0.005) sec^{-1} for the eosin data at 20 °C and (0.0020 ± 0.0016) sec^{-1} for the fluorescein data at 15 °C. We have shown that k_r increases with temperature (*13*). The ionic strength-independent value of k_r at 20 °C predicted from the fluorescein estimate at 15 °C (0.002 s^{-1}) with the published Arrhenius activation energy (29 ± 2 kcal mol^{-1}) is 0.005 s^{-1}, in satisfactory agreement with the value estimated from the ionic-strength dependence of k_{obs} at 20 °C reported by eosin. The slopes of the solid and dashed lines in Figure 8, which correspond to the changes of k_r reported by fluorescein (0.000 46 ± 0.000 01 mM^{-1} sec^{-1}) and of k_{obs} reported by eosin (0.000 52 ± 0.000 02 mM^{-1} sec^{-1}) with μ, are also similar. Therefore, the increase in k_{obs} with $[Na^+]$ observed in the "ionic-strength-jump experiments" with eosin (*11*) confirms that the rate of the change from E_K to E_{Na} is accelerated by increasing μ and is not evidence for an increase in the E_K to E_{Na} rate caused by Na^+ binding to a site that does not bind Rb^+ (*11*) or K^+ as assumed in the "induced-fit" mechanism (*12*).

Ionic strength was also jumped, along with the Na^+, Cl^-, Na,K-ATPase, ATP, and RH421 concentrations, in the titration with Na^+ that led to rejection of the concerted mechanism and postulation of an "induced-fit" alternative (*12*). In the titration with Na^+ shown in Figure 4A of the cited paper, 40 μg mL^{-1} membrane protein and 150 nM RH421 in 25 mM histidine buffer containing 0.1 mM EDTA titrated to pH 7.4 at 24 °C was mixed with an equal volume of the same buffer containing 2 mM Tris-ATP and from 0 to 600 mM NaCl. As a result, μ increased nearly an order of magnitude from about 36 to 336 mM. The value of $1/\tau$ increased from about 10 to 52 s^{-1} or roughly 5-fold compared to an approximately 7.5-fold increase in $1/\tau$ over the same ionic strength range calculated from the slopes of the lines in Figure 8 for the reaction reported by either fluorescein or eosin in the absence of ATP. Therefore, the simplest explanation of the increase in $1/\tau$ observed in the ionic-strength-jump experiments with RH421 is that the rate constant for the change from E_K to E_{Na} also increases with μ when ATP is bound.

Instead, the increase in $1/\tau$ reported by RH421 was attributed to a conformational change induced by Na^+ binding because the plot of $1/\tau$ versus the salt concentration was nonlinear (*12*). A plausible alternative explanation for apparent saturation is that a decrease in the fraction of pump molecules with substrate bound as μ increased accounted for the observed leveling off of the rate because ATP binding accelerates the change from E_K to E_{Na} (*31*), asymptotically approaching a maximum rate when the nucleotide sites are saturated (*30*). ATP binding has not been studied as a function of μ, but inverse dependence of the affinity on μ is likely because ATP is negatively charged at neutral pH and there are several positively charged amino acids in the nucleotide-binding site of Ca-ATPase (*3*). Assuming an increase in the ATP dissociation constant per order-of-magnitude increase in μ comparable to the observed (Table 1) increases in K_{Na} and K_K (3-fold) and using a published ATP dissociation constant of 0.14 ± 0.02 mM for a median μ of 106 mM (*32*) to estimate the fraction of nucleotide sites filled gives percentages of 88% near the middle and about 70% near the end of the Na^+ and ATP-jump titration on which the "induced-fit" mechanism is based (*12*). Therefore, the predicted resultant of direct dependence of the rate constant and inverse dependence of ATP binding on μ is hyperbolic-dependence of the observed $1/\tau$ on μ resembling the published titration curve (*ibid*., Figure 4A).

Implications for Molecular Mechanism. We are unaware of any precedent for ionic strength affecting a conformational

change in a protein. However, a number of cases in which μ affected protein association−dissociation reactions were documented in recent years (*33*−*35*). Ionic-strength dependence was considered diagnostic for electrostatic contributions to the interaction energy, and specific amino acids involved in ion-pair formation were identified by site-directed mutagenesis. In the majority of cases, the association rate depended inversely upon μ and the rate of the dissociation reaction depended directly upon μ, indicating interaction between proteins with unlike net charges. The larger effects of ionic strength on the association rate constant than on the dissociation rate constant generally observed in bimolecular reactions between proteins were interpreted as evidence for a two-step mechanism in which specific bonds form after a diffusion-controlled encounter complex (*36*).

The effect of ionic strength on the rate of reactions between ions in solution is discussed in textbooks on chemical kinetics (e.g., ref *25*). Equation 6 is an approximate expression relating the second-order rate constant (k) to the second-order rate constant at infinite dilution (k_∞) assuming a mean value for the closest distance of approach of the reactants.

$$\log k \cong \log k_o + 1.018 Z_A Z_B \sqrt{\mu} \qquad (6)$$

In eq 6, Z_A and Z_B are the charges on the reactants. Equation 6 was derived (*37*) by modifying an equation for the number of collisions between two molecules in solution because of Brownian motion, which gives the diffusion-controlled limit for uncharged molecules, to take into account interionic forces. The inset of Figure 7 shows that the logarithm of the first-order rate constant for the change from E_{Na} to E_K depended inversely upon the square root of μ as predicted by eq 6 for bimolecular reactions when Z_A and Z_B have opposite signs. The first-order rate constant at infinite dilution calculated from the intercept on the ordinate axis is 565 ± 1 s^{-1}. Therefore, the second-order rate constant calculated by assuming a molecular weight of 147 kD (1.1×10^9 M^{-1} sec^{-1}) approaches a value (7×10^9 M^{-1} sec^{-1}) often quoted as the diffusion-controlled limit (*38*). The estimate of the second-order rate constant for domain movement from our data is a lower limit because only about half of the enzyme purified by SDS extraction (*39*) forms phosphoenzyme. One puzzle posed by the closed Ca^{2+}-free structure of Ca-ATPase (*4*) is how the γ phosphate is transferred to the enzyme because the distance from the nucleotide-binding site to the phosphorylation site (~19 Å) is greater than the longest dimension of ATP (~13 Å). A proposed solution is that Brownian motion of the nucleotide domain transiently shortens the distance enough for phosphoryl group transfer to the aspartyl acceptor in the phosphorylation domain (*40*). Although our results show that the speed of domain movement in the E_{Na} to E_K direction is consistent with Brownian motion, the mechanism of the conformational change is inconsistent with continuous movement of the domains instead of "a deliberate conformational change" (*40*) because the conformational change in the sodium pump is only observed when two K^+ sites are filled, explaining the stoichiometry of K^+ transport (*7*).

The rate at which the closed conformation of Na,K-ATPase reverts back to the open conformation is much slower than diffusion controlled. The rate constant for the change from E_K to E_{Na} depended directly upon μ with an estimated value when $\mu = 0$ of $(2.0 \pm 1.6) \times 10^{-3}$ sec^{-1}, compared to rate constants in the range of 10^9−10^{12} sec^{-1} for diffusion-controlled reactions (*38*). Inverse dependence of domain association on μ and direct dependence of domain separation on μ are consistent with electrostatic interaction between domains with net charges of opposite sign. Nearly a diffusion-controlled rate in the association direction and much slower separation of the domains implies a minimal two-step mechanism, in which formation of an encounter complex is rate-limiting in one direction and bond cleavage is rate-limiting in the other direction.

$$E_{Na} \underset{k_{-ec}}{\overset{k_{ec}}{\rightleftharpoons}} E^{ec} \underset{k_{-bd}}{\overset{k_{bd}}{\rightleftharpoons}} E_K \qquad (7)$$

In eq 7, E^{ec} is the encounter complex formed at a diffusion-controlled rate between the domains of the enzyme. The rate constants are for formation of the encounter complex (k_{ec}), separation of the domains (k_{-ec}), stabilization of the closed structure by specific bonding between the domains (k_{bd}), and disruption of the interdomain interactions (k_{-bd}). In the steady state, eq 8 is the observed rate constant in the forward direction and eq 9 is the observed rate constant in the reverse direction (*37*).

$$k_f = \frac{k_{ec} k_{bd}}{k_{-ec} + k_{bd}} \cong k_{ec} \qquad (8)$$

$$k_r = \frac{k_{-bd} k_{-ec}}{k_{-ec} + k_{bd}} \cong k_{-ec} \frac{k_{-bd}}{k_{bd}} \qquad (9)$$

When $k_{bd} \gg k_{-ec}$, the forward reaction is diffusion-controlled and the forward rate constant is approximately the probability of the domains colliding (k_{ec}). The back reaction may be much slower than diffusion-limited separation of charged molecules, if E_K is stabilized by multiple or strong interactions between the domains ($k_{bd} > k_{-bd}$). It has been known since one of the earliest studies of the conformational change in the sodium pump in which intrinsic fluorescence was followed (*31*) that ATP binding with fractional millimolar dissociation constant accelerates the rate of the E_K to E_{Na} reaction more than 100-fold with a saturating first-order rate constant in the range of 16−54 s^{-1} depending upon the experimental protocol (*30*). However, even with this acceleration, the change from closed to open conformation is likely to remain rate-limiting for the back half of the reaction cycle because the rate constant for dephosphorylation of the K^+ conformation estimated from ^{18}O exchange measurements (*41*) is nearly an order of magnitude larger (~5×10^2 sec^{-1}) than the reported upper limit for the rate constant of the ATP-accelerated E_K to E_{Na} transition. Both K_K and K_{Na} in bold in Table 1 depend directly upon μ, as expected for binding to sites with a net negative charge, because increased shielding accelerates dissociation from the enzyme and decelerates association of the ions with the enzyme.

The Debye−Hückel equation for the activity coefficient of an ion in an electrolytic solution that was used in the derivation of eq 6 assumes that the solvent is continuous, i.e., unstructured (*37*). Therefore, it may seem surprising that eq 6 empirically describes the ionic-strength dependence of the rate constant for the change from the Na^+ to the K^+ conformation of the sodium pump. The structure of the

sodium pump has not been solved, but the Ca^{2+}-bound (*3*) and Ca^{2+}-free (*4*) structures of the calcium pump illustrate the plausibility of the conclusions drawn from kinetic studies of the conformational change in Na,K-ATPase. The nucleotide domain rotates nearly 90° toward the membrane surface, and the N-terminal or A domain rotates approximately 110° about an axis roughly normal to the membrane, when the conformation changes from open to closed (*ibid*., Figure 1). There is also lateral movement of the cytosolic domains with the phosphorylation domain moving about 23 Å in the C- to N-terminal transmembrane-helix direction and tilting approximately 30° with respect to the membrane surface as the helices rearrange in the membrane. Consistent with rate limitation by the closed to open transition in the second step of eq 7 requiring disruption of interdomain bonds (k_{-bd}), Swiss Protein Data Bank Viewer (DeepView) computes 7 hydrogen bonds (2.73−3.26 Å) between amino acids from different domains in the closed 3.1 Å structure of Ca^{2+}-free Ca-ATPase (*4*), including at least 1 and probably 2 with oppositely charged proton donor and acceptor (ion pairs). Even when neither donor nor acceptor is formally charged, hydrogen bonds can be treated approximately as electrostatic interactions between permanent dipoles (*42*). For comparison, 15 hydrogen bonds form at the interface between the rRNase domain of colicin E3 and immunity protein Im3, which dissociates with a first-order rate constant of $1.5 \pm 0.1 \times 10^{-4}$ sec^{-1} (*43*), an order of magnitude smaller than the value that we estimated for the change from E_K to E_{Na} in Na,K-ATPase ($2.0 \pm 1.6 \times 10^{-3}$ sec^{-1}). All but one of the hydrogen-bond donor−acceptor pairs in the closed conformation of Ca-ATPase are far apart (12−62 Å) in the open 2.6 Å Ca^{2+}-bound conformer (*3*); therefore, treating the solvent between them as a continuum may not be unreasonable. Therefore, the open and closed crystal structures of Ca-ATPase strengthen the kinetic evidence for electrostatic interactions between sodium pump domains and predict similar kinetic results for the calcium pump, which has not been studied as a function of μ.

Conversely, the kinetic results obtained with Na,K-ATPase predict electrostatic attraction between the domains and stabilization of E_K analogous to the computed interactions for the Ca^{2+}-free Ca-ATPase structure. To test these predictions and identify amino acids responsible for the empirical dependence of the conformational change in Na,K-ATPase on μ, the primary structure of pig Na,K-ATPase used in the stopped-flow experiments was threaded into the tertiary structures of Ca-ATPase in the Ca^{2+}-bound and Ca^{2+}-free conformations. DeepView computes the same number of interdomain hydrogen bonds for a model of the closed conformation of the pig sodium pump (7 including 1 ion pair) as it does for the closed structure of the calcium pump, but only two of the interactions are conserved. The model is based on a MSA that aligned the six signature sequences for P-type pumps (*44*) and produced models of both conformations of the enzyme (Figure 9). One conserved hydrogen bond connects backbone atoms of the N-terminal and phosphorylation domains. The donor atom is the nitrogen of valine (V717) in the signature DGVND sequence, and the acceptor atom is the backbone oxygen of a conserved serine (S215) that is three amino acids before the signature TGES sequence. The acceptor in the other conserved interaction, which joins the phosphorylation and nucleotide domains, is the backbone oxygen of a conserved glycine (G544) in the nucleotide domain, but the donor is a side-chain hydroxyl group. There is independent evidence from site-directed mutagenesis that the hydroxyl group of the conserved threonine four amino acids after the signature MV-(I)TGD sequence in P-type pumps is important for function. We found that phosphorylation of the conservative serine mutant of the threonine corresponding to T621 (pig) in human Na,K-ATPase by P_i resembled the wild-type enzyme, whereas ^{18}O exchange could not be detected when threonine was changed to valine (*45*). The specific donor−acceptor pairs that connect the nucleotide and N-terminal domains in the Ca^{2+}-free conformation of the calcium pump are not conserved. However, DeepView predicts alternative hydrogen bonds in the E_K conformer of the sodium pump. Figure 9 shows why predicting the amino acids that connect the nucleotide and N-terminal domains is particularly speculative. Homology models of the open (Figure 9A) and closed (Figure 9B) conformations of Na,K-ATPase (colored ribbons) are superimposed upon the Ca-ATPase structures (white ribbons) with sequences in the sodium pump that could not be built into the experimental electron-density maps because of gaps in the alignment colored red. To obtain a model of the closed conformation, we had to manually edit the MSA by moving a single amino acid gap in the Ca-ATPase sequence five positions upstream (see the Experimental Procedures). One measure of the lower quality of the resulting model of the closed conformation is that the calculated total energy (16.7×10^3 kcal mol^{-1}) was an order of magnitude greater than the energy calculated for the open model (1.5×10^3 kcal mol^{-1}). Two of the amino acids in the nucleotide domain of Ca-ATPase that hydrogen bond to the N-terminal domain are in a turn near the middle of a long loop that includes the edited alignment. The surface of the nucleotide domain of Ca-ATPase contacting the N-terminal domain is completed by a turn in another long loop containing serine hydrogen bonded to the N-terminal domain. The amino acids occupying similar positions in the nucleotide domain of Na,K-ATPase (N481 and D573) are rendered by balls and sticks in Figure 9 to indicate that DeepView computes bonds to a proton donor in the N-terminal domain (R238). However, both predictions require independent confirmation because the loop containing D573 had to be almost entirely rebuilt (predominantly red) and N481 is in the middle of a rebuilt (red) turn. The third predicted hydrogen bond between amino acids in the nucleotide (R428) and N-terminal (K210) domains of the sodium pump has no precedent in the calcium pump. The homology model of the sodium pump also predicts an interaction (double hydrogen bond) between amino acids in the phosphorylation (Q742) and membrane (S153) domains that is not observed in the closed structure of Ca-ATPase. However, lateral movement and tilting of the phosphorylation domain relative to the transmembrane helices occurs through a solvent-filled cavity between the phosphorylation domain and second membrane helix (M2) from the N terminus containing S153 (cf. parts A and B of Figure 9) in the space-filled homology models (not shown) that could be affected by μ. Torque supplied by bending transmembrane helices, especially M5, which extends into the phosphorylation domain, may contribute along with electrostatic interactions to the driving force for the conformational change in P-type pumps (*4*) with the

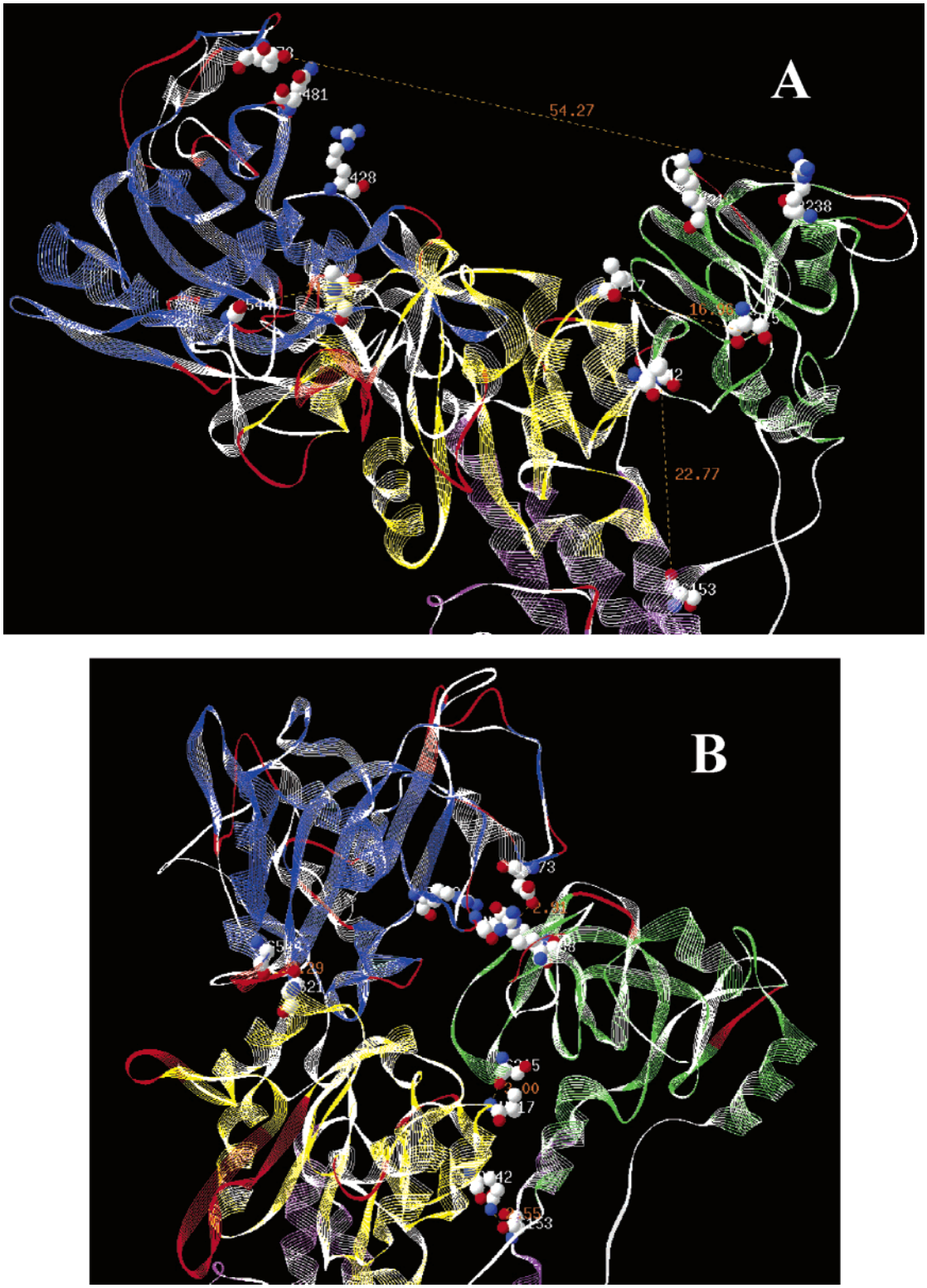

FIGURE 9: Homology model of the sodium pump. An edited MSA of pig Na,K-ATPase (target) was submitted to the Swiss-model server (see the Experimental Procedures). (A) Template 2.6 Å resolution structure of SERCA1 with Ca^{2+}-bound (1EUL). (B) Template 3.1 Å resolution structure of Ca^{2+}-free SERCA1 with thapsigargin (not shown) bound (1IWO). Ribbon renderings of the open (A) and closed (B) models of Na,K-ATPase (colored) are superimposed upon the open and closed conformations of Ca-ATPase (white). The domains of the sodium pump are colored green (N terminal), purple (membrane), yellow (phosphorylation), and blue (nucleotide), with rebuilt loops that fit the electron-density map poorly colored red. The molecules are oriented with the membrane approximately parallel to the horizontal dimension of the picture (cf. Figure 1 in ref *4*) with only the tops of some of the transmembrane helices shown. The N-terminal 37 amino acids of the sodium pump are also missing. Proton donor and acceptor amino acids predicted for Na,K-ATPase are rendered by ball-and-stick models with white labels, and one distance in angstroms between hydrogen-bonded donor and acceptor atoms in each pair of domains (N-terminal R238−nucleotide D573, phosphorylation T621−nucleotide G544, N-terminal S215−phosphorylation V717, and phosphorylation Q742−membrane S153) is shown in orange.

caution that some of the curvature observed in the closed conformation of Ca-ATPase may result from stabilization of the structure by thapsigargin bound between M3 and M5.

Differences between interdomain contacts in the calcium and sodium pumps were not unexpected because of the more than 2 orders of magnitude difference in the rate constant (k_r) for the closed to open transition in the sodium ($0.13 \pm 0.03\ s^{-1}$) and proton ($29 \pm 6\ s^{-1}$) pumps (*13*). In addition to interdomain electrostatic forces and torque supplied by intradomain rearrangements, water, which is not shown in the structures of Ca-ATPase, also must play an important role in the energetics of the conformational change in P-type pumps. Studies of the temperature dependence of the conformational change in Na,K-ATPase (*13*) showed that the units of the rate constants in Table 1 would be per day instead of per second, if the enthalpy barrier to the reaction ($\Delta H^{\ddagger} \cong 21$ kcal mol^{-1} in the E_{Na} to E_K direction) was not reduced by an entropy increase ($\Delta S^{\ddagger} \cong 23$ eu), presumably because water molecules are released from the domain surfaces in the transition-state/encounter complex. A corollary of the conclusion that electrostatic attraction accelerates domain association (eq 8) is that electrostatic repulsion when negatively charged ATP binds with low affinity to the closed conformation of the sodium pump may contribute to accelerated domain separation. The overall reaction in the E_{Na} to E_K direction is exergonic and enthalpy-driven (*13*), consistent with a more ordered E_K structure ($\Delta S° < 0$) stabilized by additional and/or stronger bonds ($\Delta H° < 0$). Evidence against (*46*) the widely held belief that tighter binding of Na^+ than K^+ to E_{Na} helps drive the sodium pump in the physiological direction (e.g., see ref *47*) is refuted by the estimates of K_{Na} and K_K in Table 1.

Added Note. While this manuscript was in preparation, a theoretical paper incorporating the "induced-fit" mechanism was published (*48*). Literature data for the rate of ATP hydrolysis as a function of [Na^+] and [K^+] (*49*) was simulated with equations for rate-determining steps in the sodium-pump cycle containing 20 arbitrary parameters. The value of computer simulations depends on the quality of the fit, the numbers used for the parameters, and the assumptions made in deriving the equations used in the analysis. There appear to be only two runs in the best fit obtained with values mainly from the RH421 literature (*ibid.*, Figure 2). All of the calculated values at low Na^+ (high K^+) are below the experimental points, and all of the calculated values at high Na^+ (low K^+) appear to be above the experimental points, except for the value (100%) used to normalize the data. The estimates used in the simulation for K_{Na} (8 mM) and K_K (10 mM) are approximately the same in disagreement with work from other laboratories indicating that $K_{Na}/K_K < 0.5$ (*49*), when determined by a variety of totally independent methods ranging from measurements of Na^+ efflux from red blood cells (*50*) to our stopped-flow studies with RH421 and other fluorescent probes (*9*). The value of 8 mM for K_{Na} was estimated with an equation that assumes three Na^+ ions bind anticooperatively (*32*). In our hands, stopped-flow data for the sodium pump are not good enough to distinguish between two and three metal-binding sites, but sequential mechanisms can be ruled out (see ref *7* and Figure 4a). This paper shows that the evidence for the "induced-fit mechanism", which was used to derive one of the equations in the computer simulation, is probably an artifact of poor experimental design.

ACKNOWLEDGMENT

The authors are indebted foremost to Dr. Lorenza Bordoli of the Swiss Institute of Bioinformatics at the Biozentrum der Universität Basel for the homology model of the closed conformation of the sodium pump. We are also indebted to Irina N. Smirnova, for technical assistance with the measurements, Dr. David Keire, also at CURE, and Professor José Cavieres of the University of Leicester in England, who read the manuscript carefully and made valuable suggestions.

REFERENCES

1. Albers, R. W. (1967) Biochemical aspects of active transport, *Annu. Rev. Biochem. 36*, 727−756.
2. Post, R. L., Hegyvary, C., and Kume, S. (1972) Activation by adenosine triphosphate in the phosphorylation kinetics of sodium and potassium ion transport adenosine triphosphatase, *J. Biol. Chem. 247*, 6530−6540.
3. Toyoshima, C., Nakasako, M., and Ogawa, H. (2000) Crystal structure of the calcium pump of sarcoplasmic reticulum at 2.6 Å resolution, *Nature 405*, 647−655.
4. Toyoshima, C., and Nomura, H. (2002) Structural changes in the calcium pump accompanying the dissociation of calcium, *Nature 418*, 605−611.
5. Robinson, J. D., and Pratap, P. E. (1993) Indicators of conformational changes in the Na^+/K^+-ATPase and their interpretation, *Biochim. Biophys. Acta 1154*, 83−104.
6. Heyse, S., Wuddel, I., Apell, H.-J., and Stürmer, W. (1994) Partial reactions of the Na,K-ATPase: Determination of rate constants, *J. Gen. Physiol. 104*, 197−240.
7. Smirnova, I. N., Lin, S.-H., and Faller, L. D. (1995) An equivalent site mechanism for Na^+ and K^+ binding to sodium pump and control of the conformational change reported by fluorescein 5′-isothiocyanate, *Biochemistry 34*, 8657−8667.
8. Smirnova, I. N., and Faller, L. D. (1995) Mechanism of the conformational change in sodium pump reported by eosin, *Biochemistry 34*, 13159−13169.
9. Lin, S.-H., Smirnova, I. N., Kasho, V. N., and Faller, L. D. (1997) Eosin, energy transfer, and RH421 report the same conformational change in sodium pump as fluorescein, *Ann. N.Y. Acad. Sci. 834*, 442−444.
10. Lin, S.-H., and Faller, L. D. (1996) Estimation of the distance change between cysteine-457 and the nucleotide binding site when sodium pump changes conformation from E_1 to E_2 by fluorescence energy transfer measurements, *Biochemistry 35*, 8419−8428.
11. Esmann, M. (1994) Influence of Na^+ on conformational states in membrane-bound renal Na,K-ATPase, *Biochemistry 33*, 8558−8565.
12. Humphrey, P. A., Lüpfert, C., Apell, H.-J., Cornelius, F., and Clarke, R. J. (2002) Mechanism of the rate-determining step of the Na^+,K^+-ATPase pump cycle, *Biochemistry 41*, 9496−9507.
13. Faller, L. D., Diaz, R. A., Scheiner-Bobis, G., and Farley, R. A. (1991) Temperature dependence of the rates of conformational changes reported by fluorescein 5′-isothiocyanate modification of H^+,K^+- and Na^+,K^+-ATPases, *Biochemistry 30*, 3503−3510.
14. Xu, K. (1989) Any of several lysines can react with 5′-isothiocyanatofluorescein to inactivate sodium and potassium ion activated adenosinetriphosphatase, *Biochemistry 28*, 5764−5772.
15. Lin, S.-H., and Faller, L. D. (2000) Preparation of Na,K-ATPase specifically modified on the anti-fluorescein antibody-inaccessible site by fluorescein 5′-isothiocyanate, *Anal. Biochem. 287*, 303−312.
16. Lin, S.-H., and Faller, L. D. (1993) Time resolution of fluorescence changes observed in titrations of fluorescein 5′-isothiocyanate-modified Na,K-ATPase with monovalent cations, *Biochemistry 32*, 13917−13924.
17. Abbott, A. J., Amler, E., and Ball, W. J., Jr. (1991) Immunochemical and spectroscopic characterization of two fluorescein 5′-isothiocyanate labeling sites on Na^+,K^+-ATPase, *Biochemistry 30*, 1692−1701.

18. Smirnova, I. N., and Faller, L. D. (1993) Role of Mg^{2+} ions in the conformational change reported by fluorescein 5′-isothiocyanate modification of Na^+,K^+-ATPase, *Biochemistry 32*, 5967−5977.
19. Faller, L. D., Smirnova, I. N., Lin, S.-H., and Stengelin, M. (1994) Mechanism of the conformational change in fluorescein 5′-isothiocyanate-modified Na^+/K^+-ATPase, in *The Sodium Pump: Structure Mechanism, Hormonal Control, and Its Role in Disease* (Bamberg, E., and Schoner, W., Eds.) pp 593−604, Steinkopff, Darmstadt, Germany.
20. Brooks, S. P. J., and Storey, K. B. (1992) Bound and determined: A computer program for making buffers of defined ion concentrations, *Anal. Biochem. 201*, 119−126.
21. Good, N. E., Winget, D., Winter, W., Connolly, T. N., Izawa, S., and Singh, R. M. M. (1966) Hydrogen ion buffers for biological research, *Biochemistry 5*, 467−477.
22. Glantz, S. A., and Slinker, B. K. (1990) Regression with two or more independent variables, in *Primer of Applied Regression and Analysis of Variance*, pp 50−104, McGraw−Hill, New York.
23. Smirnova, I. N., and Faller, L. D. (1993) Mechanism of K^+ interaction with fluorescein 5′-isothiocyanate-modified Na^+,K^+-ATPase, *J. Biol. Chem. 268*, 16120−16123.
24. Bass, M. B., and Fromm, H. J. (1985) *trans*-1,2-Diaminocyclohexane-*N*,*N*,*N*′,*N*′-tetraacetic acid is superior to ethylenediamine-*N*,*N*,*N*′,*N*′-tetraacetic acid for sequestering Mg^{2+} in ^{31}P NMR experiments involving ATP spectra at neutral and acidic pH, *Anal. Biochem. 145*, 292−301.
25. Frost, A. A., and Pearson, R. G. (1953) Influence of ionic strength, in *Kinetics and Mechanism*, pp 138−142, John Wiley and Son, New York.
26. Faller, L. D., Kasho, V. N., Smirnova, I. N., Lin, S.-H., and Farley, R. A. (2000) The catalytic domain of P-type pumps: Evidence for two nucleotide sites, in *Excerpta Medica International Congress Series 12007: Na/K-ATPase and Related ATPases* (Taniguchi, K., and Kaya, S., Eds.) pp 389−396, Elsevier, Amsterdam, The Netherlands.
27. Edsall, J. T., and Wyman, J. (1958) Polybasic acids, bases, and ampholytes, including proteins, in *Biophysical Chemistry*, Vol. 1, pp 477−485, Academic Press, New York.
28. Karlish, S. J. D. (1980) Characterization of conformational changes in (Na,K)ATPase labeled with fluorescein at the active site, *J. Bioenerg. Biomembr. 12*, 111−136.
29. Skou, J. C., and Esmann, M. (1983) The effects of Na^+ and K^+ on the conformational transitions of (Na^+ + K^+)-ATPase, *Biochim. Biophys. Acta 746*, 101−113.
30. Steinberg, M., and Karlish, S. J. D. (1989) Studies of conformational changes in Na,K-ATPase labeled with 5-iodoacetamidofluorescein, *J. Biol. Chem. 264*, 2726−2734.
31. Karlish, S. J. D., and Yates, D. W. (1978) Tryptophan fluorescence of Na^+,K^+-ATPase as a toll for study of the enzyme mechanism, *Biochim. Biophys. Acta 527*, 115−130.
32. Kane, D. J, Fendler, K., Grell, E., Bamberg, E., Taniguchi, K., Froehlich, J. P., and Clarke, R. J. (1997) Stopped-flow kinetic investigations of conformational changes of pig kidney Na^+,K^+-ATPase, *Biochemistry 36*, 13406−13420.
33. Wallis, R., Moore, G. R., James, R., and Kleanthous, C. (1995) Protein−protein interactions in colicin E9 DNase-immunity protein complexes. 1. Diffusion-controlled association and femtomolar binding for the cognate complex, *Biochemistry 34*, 13743−13750.
34. Schreiber, G., and Fersht, A. R. (1993) Interaction of barnase with its polypeptide inhibitor barstar studied by protein engineering, *Biochemistry 32*, 5145−5150.
35. Escobar, L., Root, M. J., and MacKinnon, R. (1993) Influence of protein surface charge on the bimolecular kinetics of a potassium channel peptide inhibitor, *Biochemistry 32*, 6982−6987.
36. Zhou, H.-X. (2001) Disparate ionic-strength dependencies of on and off rates in protein−protein association, *Biopolymers 59*, 427−433.
37. Eigen, M., Kruse, W., Maass, G., and DeMaeyer, L. (1964) Rate constants of protolytic reactions in aqueous solution II the maximum rate of ionic recombination in solution, *Prog. React. Kinet. 2*, 287−296.
38. Fersht, A. (1977) Upper limits on rate constants: Association and dissociation, in *Enzyme Structure and Mechanism*, 2nd edition, pp 147−148, W. H. Freeman and Company, New York.
39. Jørgensen, P. L. (1974) Purification and characterization of (Na^+ + K^+)-ATPase. 3. purification from the outer medulla of mammalian kidney after selective removal of membrane components by sodium dodecyl sulfate, *Biochim. Biophys. Acta 356*, 36−52.
40. Xu, C., Rice, W. J., He, W., and Stokes, D. L. (2002) A structural model for the catalytic cycle of Ca^{2+}-ATPase, *J. Mol. Biol. 316*, 201−211.
41. Farley, R. A., Heart, E, Kabalin, M., Putnam, D., Wang, K., Kasho, V. N., and Faller, L. D. (1997) Site-directed mutagenesis of the sodium pump: Analysis of mutations to amino acids in the proposed nucleotide binding site by stable oxygen isotope exchange, *Biochemistry 36*, 941−951.
42. Creighton, T. E. (1984) The physical nature of noncovalent interactions, in *Proteins: Structures and Molecular Properties*, pp 134−139, W. H. Freeman and Company, New York.
43. Walker, D., Moore, G. R., James, R., and Kleanthous, C. (2003) Thermodynamic consequences of bipartite immunity protein binding to the ribosomal ribonuclease colicin E3, *Biochemistry 42*, 4161−4171.
44. Serrano, R. (1969) Structure and function of plasma membrane ATPase, *Annu. Rev. Plant Physiol. Plant Mol. Biol. 40*, 61−94.
45. Kane, D. J., Farley, R. A., Nagy, A. K., and Faller, L. D. (2002) Effects of Mutations on Mg^{2+} and P_i Binding by Na,K-ATPase, *Biophys. J. 82*, 262a.
46. Schulz, S., and Apell, H.-J. (1995) Investigation of ion binding to the cytoplasmic binding sites of the Na,K-pump, *Eur. Biophys. J. 23*, 413−421.
47. Läuger, P. (1991) Na,K-ATPase: Mechanism, kinetics, free-energy levels, electrogenic properties, in *Electrogenic Ion Pumps*, pp 177−224, Sinauer Associates, Sunderland, MA.
48. Kong, B. Y., and Clarke, R. J. (2004) Identification of potential regulatory sites of the Na^+,K^+-ATPase by kinetic analysis, *Biochemistry 43*, 2241−2250.
49. Skou, J. C. (1979) The (Na^+ + K^+) activated enzyme system and its relationship to transport of sodium and potassium, *Q. Rev. Biophys. 7*, 401−435.
50. Garay, R. P., and Garrahan, P. J. (1973) The interaction of sodium and potassium with the sodium pump in red cells, *J. Physiol. 231*, 297−325.

BI040018C